The Knee Wear Prediction of UHMWPE Tibial Insert Using VIPRO Platform

Lucian Capitanu[1], Luige Vladareanu[2] and Virgil Florescu[3]

1. Tribology Department, Institute of Solid Mechanics of the Romanian Academy, Bucharest 010141, Romania

2. Robotics and Mechatronics Department, Institute of Solid Mechanics of the Romanian Academy, Bucharest 010141, Romania

3. Mechanical Department, Institute of Civil Engineering, Bucharest 050236, Romania

Abstract: The failure mechanism was postulated as a combination of the high level of loading during normal activities and a non-conforming contact mechanism between the femoral condyles and the tibial insert. The question that arises is: could be this phenomenon evaluated quantitatively a priori, e.g., could be the failure due to delamination wear predicted? In order to do some finite element simulations were performed to dynamically determinate the contact area and contact pressure for three different activities. The results obtained using VIPRO platform lead to the conclusion that many clinically reported failures of the tibial tray are caused by the adhesive and fatigue wear.

Key words: Total knee prosthesis, wear, experimental methods, experimental trials, knee simulator, programmable logical controller, VIPRO platform.

1. Introduction

Recent clinical studies [1, 2] on massive wear of the tibial polyethylene insert caused by improper contact gear for the artificial knee joint, have shown that this is the main cause for the correction of the knee prosthesis. In Ref. [3], Knight et al. reports that in all of the 18-th worn prosthesis (out of 209 cases of primary arthroplasty for knee joint), we can observe wear pits on the surface of the tibial tray (specific to the adhesive wear) as well as delaminating.

Prosthesis life was about 80 months, close to the time reported in Ref. [4], which is 72 months. There were also studies on the massive delaminating of the polyethylene occurred earlier [5-8].

Examining an early retrieved prosthesis, Ries et al. [9] noticed gross wear pitts and delamination of the tibial insert accompanied by an increase of percentage cristalinity at a plane coincident with the plane of delamination and the presence of subsurface oxidation

peak typically observed in UHMWPE inserts, gamma-irradiated in air and aged. Still controversial, the idea that increasing the thickness of tibial inserts will reduce wear was rather false. The disputed idea that the wear of the polyethylene insert can be reduced by increasing of its thickness is rather false. In reality, the main cause of the joint wear phenomenon is represented by the high level of the superficial pressure caused by incongruent contact areas [3, 4] and the present study is based on this idea.

One starts with a close analysis of the different types of tibio-femoral prosthetic joints: fixed bearing condylar prothesis with a partial conformity between the tibial and femoral surfaces (over or exterior to the crossed posterior ligament) and mobile prosthesis with tibial component consisting in a fixed metallic tray with one/two plastic component/components defining the movement surface of the bearing.

These components can have translational and rotational movements. There were also studies on prosthesis with a rotating tray, similar to those mentioned above, but where the plastic component of the bearing fulfil only one free rotation around the

---

Corresponding author: Lucian Capitanu, professor, D.Eng., research fields: tribology, biotribology, biomechanics.

longitudinal axis, generally located in the centre.

Analyzing two retrieved TKP (after 21 and 16 years from implantation), Oonishi et al. [10] noticed the presence of parallel scratches (oriented antero-posterior) on femoral component, and large delamination of polyethylene tibial insert.

2. The Knee Contact Mechanism

Two bodies that are in contact in a point become deformed when pressed against each other, thus creating a small contact surface. Hertz has calculated the deformations and stresses in the case of homogenous, isotropic, frictionless, linear elastic bodies.

For two different materials, having the elasticity modulus E_1 and E_2, and the Poisson ratios v_1 and v_2, the equivalent elasticity modulus E is defined, through the relation (1):

$$E = \frac{E_1 E_2}{\left(1 - v_1^2\right) E_2 + \left(1 - v_2^2\right) E_1} \qquad (1)$$

For a ball on flat couple, where the ball is made out of CoCr alloy, with the elasticity modulus $E_1 = 19 \times 10^4$ N/mm^2, and the Poisson's coefficient $v_1 = 0.3$ and the plane sample made out of UHMWPE ($v_2 = 0.36$ and $E_2 = 1.06 \times 10^3$ N/mm^2), the equivalent elasticity modulus is $E = 1.21 \times 10^3$ N/mm^2.

Considering two revolution bodies having boundary surfaces with $1/R_1$ and $1/R_2$ curvatures, one introduces the relative curvature given by: if one of the surfaces is concave, the curvature of that surface will be considered negative. For the particular case of the contact between a sphere of radius r and a plane, we have:

$$\frac{1}{R} = \frac{1}{R_1} + \frac{1}{R_2} \qquad (2)$$

If one of the surfaces is concave, the curvature of that surface will be considered negative. For the particular case of the contact between a sphere of radius r and a plane, we have:

$$\frac{1}{R_1} = \frac{1}{r} \quad \text{and} \quad \frac{1}{R_2} \to 0$$

Applying an F compression load between the two parts leads to the appearance of a contact area, due to surface deformation. The F compression force causes an h movement of the center of the sphere, through its penetration in the flat body, according to relation:

$$h = \left(\frac{9F^2}{16rE^2}\right)^{1/3} \qquad (3)$$

The relation between the circle diameter l (of the spherical contact spot) and the penetration h is [11]:

$$l^2 = 4 \cdot r \cdot h$$

Using Eq. (3), it results the diameter of the contact spot:

$$l = \left(\frac{6F \cdot r}{E}\right)^{1/3} \qquad (4)$$

3. Determination of Wear Parameters

An experimental device was created for the simulation of the wear process of total knee prosthesis components. For this purpose, a ball/flat couple was used. It consists of a ball made of CoCr alloy, simulating a condyle of the femoral component, and a UHMWPE (ultra haigh molecular weight polyethylene) disk placed underneath representing the tibial component. The thickness of UHMWPE disk was 5 or 10 mm and was mounted on a CoCr alloy plate.

The movement made and the applied loadings were based on biomedical studies. The complex movement consisted in: FE (flexion-extension), APT (antero-posterior translation) and IOR (internal-external rotation). The FE movement is applied to the ball and APT and IOR to the disk (Fig. 1).

These movements were made by intermediate of a rod—handle mechanism. The movement variation in the time was almost sinusoidal, a movement cycle period being of 1 s. The kinematics is very similar to
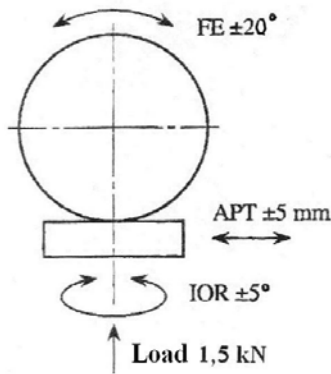
Fig. 1 The friction couple kinematics.

Fig. 2 A sample line graph using colours which contrast well both on screen and on a black-and-white hard copy.

that used by V. Saikko, T. Ahlroos and O. Calonius at the Helsinky University of Technology [12].

The amplitude of the FE movement was of 40°. For FE movement only, the sliding distance between the extreme positions would be of 20 mm, for a 54 mm diameter ball. Anyway, the APT movement with the amplitude of 10 mm, was synchronized with the FE movement so that the maximum flexion wold coincide with the maximum posterior translation of the disk, and the maximum extension with the corresponding maximum anterior translation. This has shortened the sliding distance between the extreme positions. Due to both movements, the contact spot moved relatively cyclic on the disk surface.

The rod—handle mechanism was created so the phase angle between fhe IOR and the APT sinusoidals is π/2. As a consequence, the locus of the point where the force is applied on the disk (meaning the geometrical path of a theoretical contact point) was an antisymmetrical narrow figure, in the shape of eight (Fig. 2).

The parametrical equations of the curve (C₁) are:

$$\begin{array}{l} x_1 = d \cdot k \cdot \cos(\varphi_0 \cdot k) \\ y_1 = d \cdot k \cdot \sin(\varphi_0 \cdot k) \\ k \in [0,1] \end{array} \qquad (5)$$

where, k is the dimensionalized time; d is the relative translation between the surfaces; φ_0 is the maximum IOR angle.
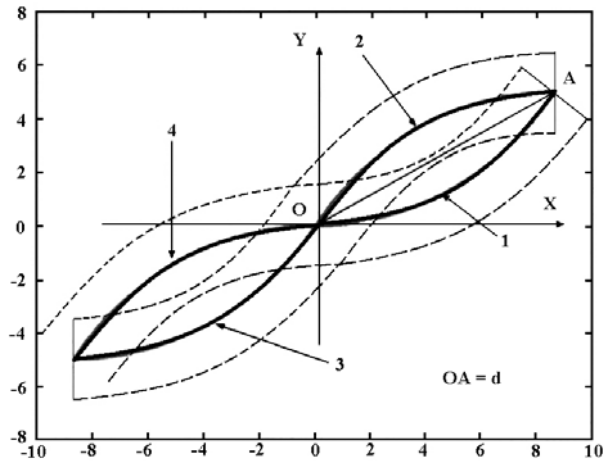
Similar, the equations of curve (C₂) are:

$$\begin{array}{l} x_2 = d \cdot \cos\varphi_0 - d \cdot k \cdot \cos(\varphi_0 \cdot k) \\ y_2 = d \cdot \sin\varphi_0 - d \cdot k \cdot \sin(\varphi_0 \cdot k) \\ k \in [0,1] \end{array} \qquad (6)$$

The curves (C₃) and (C₄) are antisymmetrically defined:

$$x_3 = -x_1, y_3 = -y_1, k \in [0,1] \qquad (7)$$

$$x_4 = -x_2, y_4 = -y_2, k \in [0,1] \qquad (8)$$

The length of one of the curves is:

$$L = \int_0^1 \sqrt{\left| \left(x_1^{'}\right)^2 + \left(y_1^{'}\right)^2 \right|} \cdot dk \qquad (9)$$

From Eq. (5), it results:

$$L = \int_0^1 \sqrt{1 + k^2} \cdot dk \qquad (10)$$

The area of the circular segment (Sw) defining the vertical profile of the wear imprint is:

$$S_w = \frac{r^2}{2} \cdot \left[\arcsin\left(\frac{l}{2r}\right) - \frac{l}{2r} \right] \qquad (11)$$

where, l is the width of the imprint.

The volume of the theoretical imprint can be calculated as:

$$V_w = 2S_w \cdot L \qquad (12)$$

The APT movement was realized so that lever fixed on the FE shaft led to a low-friction movement of a straight, horizontal beam, coupled to a force transducer. The transducer signal was proportional to the friction force between the ball and the disk. This method allows for determination of the friction coefficient μ. The first experiments carried out, using only FE and APT movements, led to a very small wear rate (Fig. 3). The wear is manifested by the appearance of wear pits on the side surfaces of the polyethylene tibial insert due to cyclic mechanical loading of UHMWPE.

By adding the IOR movement, the wear rate increased, the wear phenomenon becoming more complex. Due to the track in the shape of eight of the application point of the resulting force, it twice passes over the same spot, leading initially to wear through delamination and then breaking the tibial insert (Fig. 4).

The vertical loading of 1.5 kN was constant, corresponding to the maximum load induced in the knee by the routine activities. Due to translations, the stress in the disk modify in cyclic manner, even for a constant compression force.
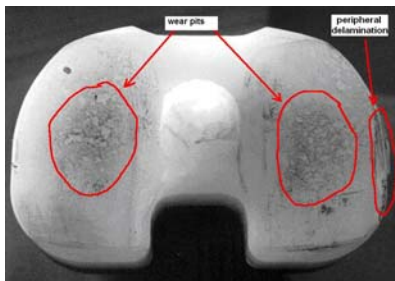

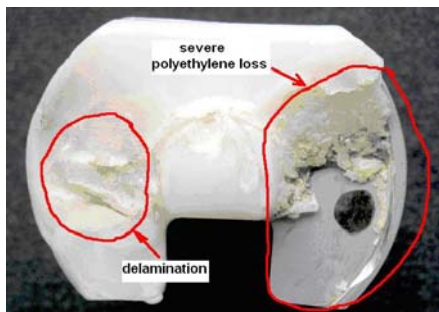**Fig. 3   The wear of tibial tray using only FE and APT movements.**

Fig. 4   The severe wear of tibial tray using only FE, APT and IOR movements.

The disk samples (having a diameter of 40 mm) were made out of very high density polyethylene, type Gur 1050. The tests were made on different disks. Oxidation was simulated through the ageing of the polyethylene after the gamma irradiation. The lower part of the disk was placed on a level support of CoCr alloy. The lubricant was sterilized, filtered physiological serum with a low content of proteins and endotoxins. The tests were carried out at the room temperature. During the tests, the value of the friction force was also achieved.

The duration of the tests was of 5×10^6 cycles, at frequency of 1 Hz. The tests were stopped every 500,000 cycles in order to change the lubricant.

The elastic deformation of the polyethylene under pressure has a consequence an increase of its radius in the contact area. By noting r—the radius of the undeformed contact area and r_m—the radius of the deformed area by the contact, that $r_m > r$, it can be seen in Fig. 5.

The equivalent curvature radius in the point where l_m imprint width was measured, can be calculate from Eq. (4):

$$r_m = \frac{E \cdot l_m^3}{6F} \qquad (13)$$

where, l_m is the measured length of the imprint.

The volume of material for the flat element, removed through wear, will be:

$$V_w = \frac{L_m \cdot r_m^2}{2} \cdot \left[\arcsin\left(\frac{l_m}{2r}\right) - \frac{l_m}{2r} \right] \qquad (14)$$

Solving numerically, one obtains the solution:
$$R_m = 27.3212 \text{ mm} \approx 1.012 \, r$$

Practically, the microscopic measurement of the imprints width in five established points, allows computation of the medium width of the imprint. Based on this value, the volume of worn material of the flat polyethylene element V_w is determined as well as medium depth of the layer removed through wear h_{wm}.
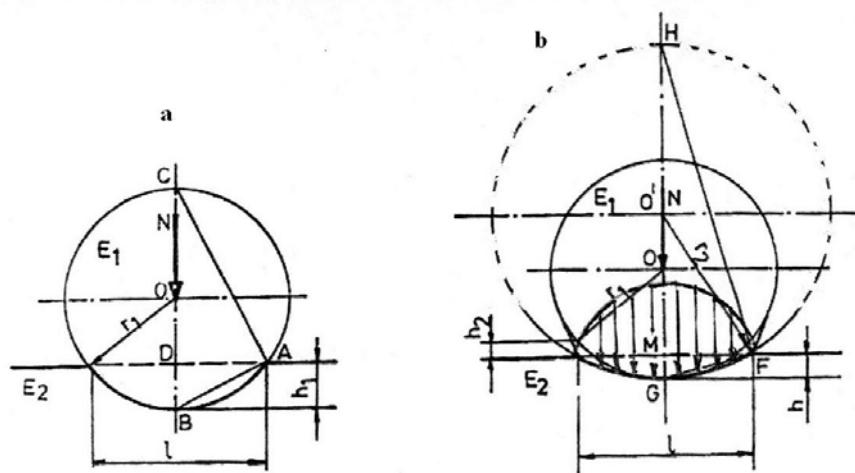
Fig. 5   Elastic deformation under load of the plane component, in the contact area: a—theoretical case and b—practical case.

4. The Knee Prosthesis Simulator Control System

Aiming to improve the performance of KPS (knee prosthesis simulator) control system, a new method has been developed for hybrid position—force control on five DOF (degrees of freedom) in an open architecture with PC interfaced multi-processor PLC system, in order to obtain new control functions. Mainly, the architecture allows for real time control, having two sources of data: measurements of dynamic forces and static precision as interaction between the work piece and environment [13, 14]. The hybrid position—force control in Cartesian coordinates, conceived as a control system in OAH (open architecture), is realized by processing in real time the Jacobean matrix obtained from kinematics through Danevit—Hartenberg method with the calculus of the inverse Jacobean matrix for back loop control [15].

The studying method is produced a control system for knee prosthesis simulator on 5 DOF which maintains a constant force of vertical pressure on the tibial component. First considered is a mathematical model determined off-line based on the studies done by the authors, from which the trajectories for femoral and tibial movement are generated online.

The trajectory of the tibial movement is controlled in real time and is composed by four movement functions corresponding to the 4 DOF. The Femoral movement trajectory, which represents the 5-th DOF, is synchronized with the tibial movement trajectory trough the freedom axis trajectory control accordingly the mathematical model determined off-line and the chosen law of movement. The control system has four KPS stations. Each station allows, individually or jointly with the others, the Cartezian force and torque $(F_x, F_y, F_z, M_x, M_y, M_z)$ to be monitored continuously or at periodical intervals, using load cess.

Supplementary, the temperatures control for 8 measurement points is available.

Hybrid position—force control of knee prosthesis equipped with compliant joints must take into consideration the passive compliance within the system [15, 16]. The generalized surface on which the knee prosthesis labours must be defined into a constraint space with five DOF, with position constraints along the normal to this surface and force constraints along the tangents.

On the basis of these two constraints, the general structure of hybrid position—force control and the general constructive scheme is presented in Figs. 6 and 7.

Out of simplification considerations, the coordinate transformations are not noted. The variables X_C and F_C represent Cartesian position, respectively the Cartesian force exerted upon environment. Considering X_C and
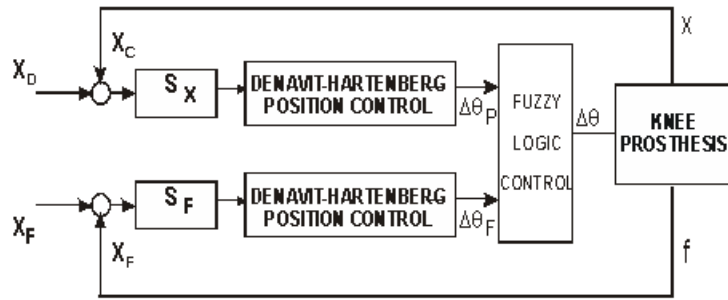
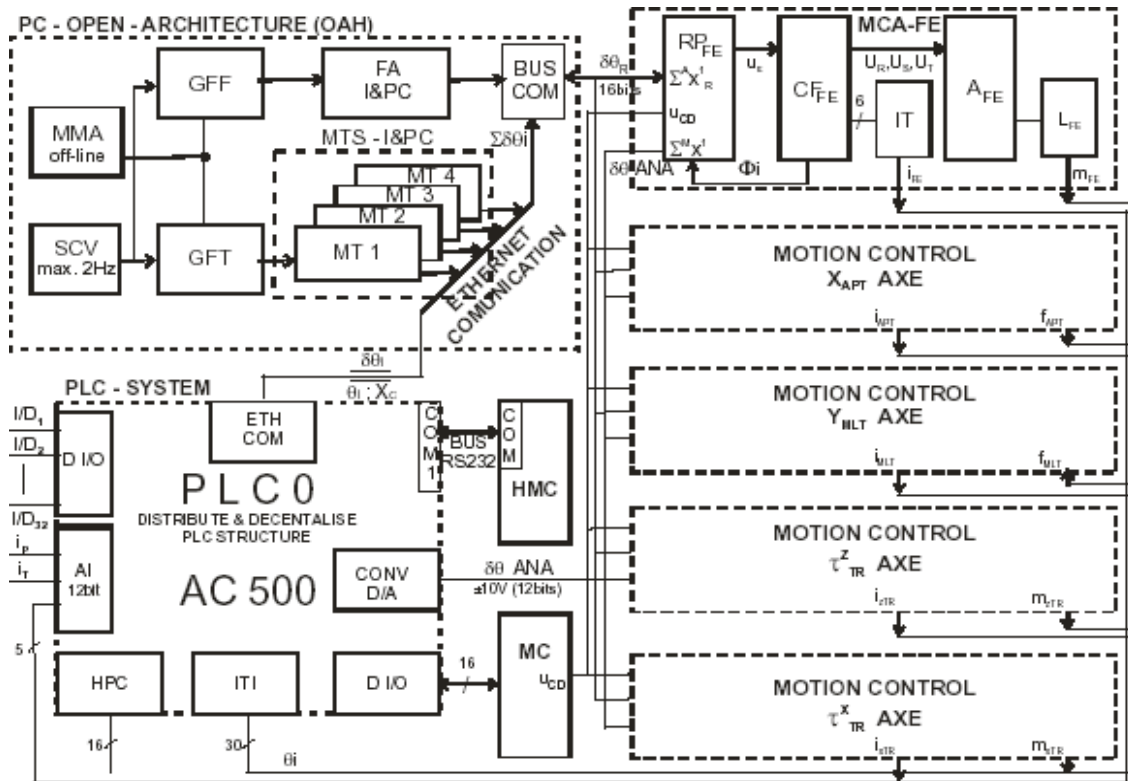**Fig. 6   The general structure for hibrid control.**

Fig. 7   Control system for knee prosthesis simulator.

F_C as expressed in environment—specific coordinates, the selection matrix S_x and S_f can be determined, which are diagonal matrixes with 0 and 1 as diagonal elements, and fulfil the relation:

$$S_x + S_f = L_d \qquad (15)$$

In more recent approaches, S_x and S_f are methodically deduced from the kinematical constraints imposed by the working environment. Let A and B be full column rank matrices spanning the wrench spaces of constraint. They satisfy the relation:

$$A \cdot B = 0 \qquad (16)$$

Then S_x and S_f can be determined through the relations:

$$S_f = \left(B^t \cdot \psi^{-1} \cdot B \right)^{-1} \cdot B^t \cdot \psi^{-1} \qquad (17)$$

$$S_x = \left(A^t \cdot \psi \cdot A \right)^{-1} \cdot A^t \cdot \psi \qquad (18)$$

where, Ψ is usually a symmetrical, positive-definite matrix. It is easily verifiable [13, 17] that using the above approaches, S_x and S_f always fulfil:

$$rang\left(S_x \right) + rang\left(S_f \right) = 6 \quad S_x' \cdot S_f = 0 \quad (19)$$

The control rules to bring to zero the position errors $e_x = \Delta\theta_P$ and force errors $e_f = \Delta\theta_F$. For an ideal system, the behaviour of knee prosthesis is defined by:

$$S_x \cdot (v_{des} - v) = 0 \qquad (20)$$

$$S_f \cdot (f_{des} - f) = 0 \qquad (21)$$

where, v is velocity, f is the force and index "*des*" specifies the reference parameter (the desired value).

Velocity constraint is the only one taken into consideration here and constraint position is satisfied as a consequence.

Eqs. (20) and (21) lead to following conclusion: with the aid of hybrid control, the knee prosthesis acts as a rigid body, without mass, submitted to an external force f_{des} and connected through an ideal kinematical constraint to another body, whose velocity is v_{des}.

A reference position interpolation for four tibial axis is provided through multi-tasking system. The experimental results are in good agreement with the theoretical predicted results for trajectory control, showing the possibility of practical implementation of control strategies for the KPS using PLCs (programmable logical controllers). The monitored parameters are available for evaluating the prosthesis materials, implant wear, change of friction rate and tribological behaviour.

The VIPRO dynamic versatile intelligent portable robot platform (Fig. 8) is developed through a multi-disciplinary concept using the 3D virtual representation with high graphic processing power and advanced programming languages through the mechanical structure modeling, an open architecture system keeping the TKP classic control system and of the intelligent control interfaces (fuzzy control, multi-agent control, dynamics and adaptive control, robust and iterative learning control, etc.) implemented through IT&C techniques on fast and high data processing.

The improvement of the VIPRO platform performances is developed through optimization of certain intelligent control methods: RNC (Robot Neutrosophic Control) known as Vladareanu-Smarandache method [19], by applying neutrosophic logic and DSmT (Dezert Smarandache Theory), representing a new theory that merges the fuzzy theories and information fusion, Human Adaptive Mechatronics method that can adapt themselves to the human's skill in various environments and provide assistance in improving performances [20], PNMCA (Petri Net and Markov Chains Approach) for motion dynamic control in a more efficient concurrency control [21]. The VIPRO
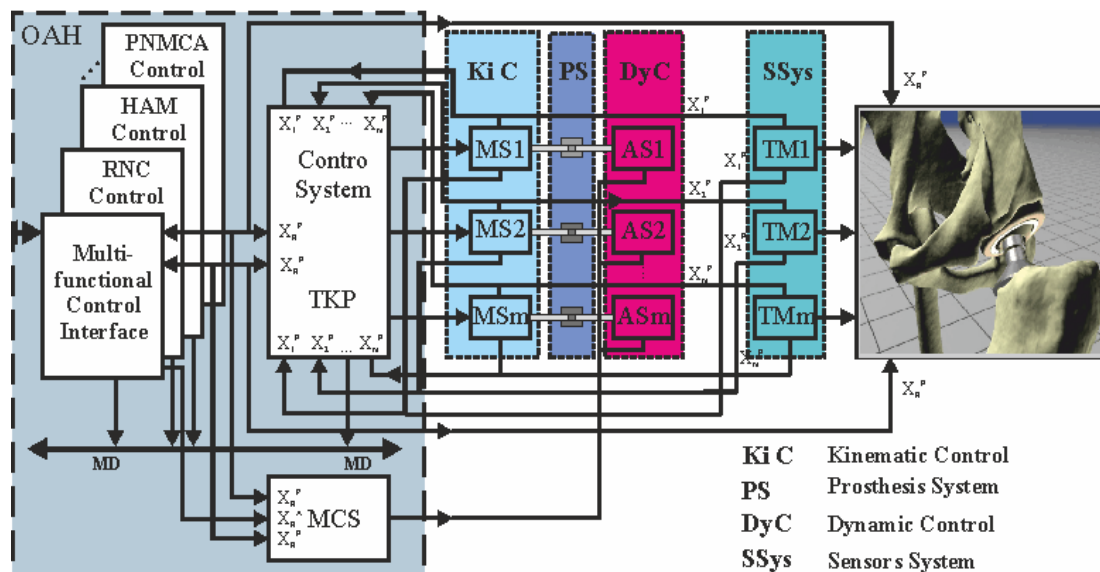

Fig. 8   Schematic representation of the VIPRO platform.

real time control system with OAH ensures flexibility, short time execution with precision targeting and repeatability of the motion and developments to increase the performances.

The novelty VIPRo platform will be able to be sold in competition with other similar virtual simulation platforms, called virtual instrumentation: CDA, CAM, CAE, Solid Works, etc., very reliable platforms in powerful modeling but only in a virtual environment, or MatLab, Simulink, COMSOL, Lab View simulation platforms allow extensions for real time data acquisition and signal processing, but none of which allow the design, testing and experiment of intelligent control methods on a real TKP control system. The VIPRO versatile intelligent portable robot platform used to the simulation and testing of the prosthetic hip or knee implants is expected to be applied in developing human aid mechatronics in various fields such as rehabilitation support and physical training support in medical field, ADL support for disabled people, rescue support at disaster sites.

The developed method is also useful for the validation of the analytical models which are to be further developed to portray the dynamic behaviour and timeline behaviour of the knee prosthesis.

Table 1 presents the results obtained from the experimental trials using VIPRO Platform, for a constant force of 1,500 N, having an FE of ±5 mm.

5. Results

The results obtained from the experimental trials using VIPRO Platform, for a constant force of 1,500 N, having an FE of ±5 mm, are presented in Table 1.

The tests 1 and 2 were performed on polyethylene disks having a 5 mm width, and tests 3, 4 and 5 on disks having 10 mm width. The theoretical length of the friction distance covered by the contact spot, on each movement cycle, was 10 mm. The measurements carried out with the microscope have shown an effective increase of these values, probably caused by the shear stresses occurred on the edges of contact area.

Table 1 Wear of polyethylene disks and average of friction coefficient.

No.	Wear	Wear factor	Wear pit dimensions			μ
			L	W	D	
1	72.26	0.935	10.3	1.32	0.6	0.036
2	128.56	1.679	10.1	1.61	1.3	0.053
3	71.31	0.914	10.4	1.31	0.5	0.035
4	120.40	1.514	10.6	1.56	0.9	0.034
5	112.48	1.428	10.5	1.52	1.0	0.047

Wear (10^{-3} mm^3); Wear factor (10^{-11} mm^3/Nm); L—Length (mm); W—Width (mm); D—Depth (10^{-3} mm)

For tests 2 and 3, the UHMWPE samples were sterilized through γ irradiation and aged through air convection.

Tests 1 and 4 were carried out the samples that were not irradiated and test 5 on samples that were irradiated but not aged. The wear factor was determined based on Archard's relation [18]:

$$V_w = F \cdot k \cdot v \cdot t \qquad (22)$$

where, V_w—volume of material removed through wear (cm^3); F—working load (daN); v—relative sliding speed (cm/s); t—test duration (h); k—wear factor (cm^3·s/daN·m·h).

Eq. (15) expresses a general law for the dependency of the wear as function of the compressive force between the bodies in contact and the space covered by friction.

Therefore, we can get:

$$V_w = F \cdot k \cdot v \cdot t \qquad (23)$$

where, L_f is the space covered by friction.

Table 1 also shows the medium values of the friction coefficient, determined based on the measurements carried out by intermediate of the force transducer coupled on the bearing with low linear friction, part of generator of the APT movement.

6. Conclusion

The fatigue wear was identified as the main phenomenon on responsible for the polyethylene tibial insert failure. Clinical studies show that even tibial

parts that are retrieved for other reasons (implant loosening, misalignment, etc.) presented markers of fatigue wear (cracks in the subsurface, wear pits, delamination, and loss of large pieces of polyethylene). The cumulative nature of the wear fatigue phenomenon requires a qualitative and quantitative evaluation of the transfer of loadings through the joint and a summation technique that is relevant for the variety of the human activities. The first part was assessed by a combination of dynamic finite element analyses of the joint contact mechanism. For the second part, we assumed that normal walking, stair ascending and stair descending were the regular activities with a dominant impact on the phenomenon.

Appreciating the wear of the tibial tray of total knee prosthesis is very difficult. Measuring the wear becomes more challenging due to polyehylene's considerable yield. It is also difficult to establish the value of the wear factor because measuring volume of material removed is also complicated to do. At the moment appreciating the wear of tibial tray through simulation is generally done using qualitative methods, based on the microscopical investigation of the wear imprints. The initial polishing of the polyethylene's contact surface is a sign certifying the adhesive nature of wear.

The tests carried out for a different number of cycles prove that the wear rate of the γ irradiated and air convection aged disks was greater in the beginning, decreasing afterwards and getting stabilized around the values of the wear rates for not irradiated specimens.

The wear rate of the γ irradiated and aged 10 mm thick disk is about twice as for those that were not irradiated. The wear rate for 5 mm aged disks is greater than that of similar disks, with a 10 mm thickness. The results obtained lead to the conclusion that many clinically reported failures of the tibial tray are caused by the mechanisms of adhesive and fatigue wear. A closer look to the distribution of damage score reveals that the maximum damage is likely to occur not at the contact surface but, rather, in the subsurface.

The presence of maxima values in an area were other studies [9] identifies an increase of the percentage cristalinity and the presence of subsurface oxidation peak induced by the gamma-irradiation and ageing of the prosthesis could be an explanation of the early delamination of the polyethylene inserts.

References

[1] Blunn, G. W., Joshi, A. B., Minns, R. J., Lidgren, L., Lilley, P., Ryd, L., Engelbrecht, E., and Walker, P. S. 1997. "Wear in Retrieved Condylar Knee Arthroplasties." *Journal of Arthroplasty* 12: 281-90.

[2] Wasielewski, R. C., Galante, J. O., Leighty, R. M., Natarajan, R. N., and Rosenberg, A. G. 1994. "Wear Patterns on Retrieved Polyethylene Tibial Inserts and Their Relationship to Technical Considerations during Total Knee Arthroplasty." *Clinical Orthopaedic* 299: 31-43.

[3] Knight, J. L., Gorai, P. A., Atwater, R. D., and Grothaus, L. 1995. "Tibial Polyethylene Failure after Primary Porous-Coated Anatomic Total Knee Arthroplasty." *Journal of Arthroplasty* 10: 748-57.

[4] Heck, D. A., Clingman, J. K., and Kettelkamp, D. G. 1992. "Gross Polyethylene Failure in Total Knee Arthroplasty." *Orthopedics* 15: 23-8.

[5] Engh, G. A., Dwyer, K. A., and Hanes, C. K. 1992. "Polyethlyene Wear of Metal-Backed Tibial Components in Total and Unicompartmental Knee Prostheses." *J. Bone Joint Surg.* 74B: 9-17.

[6] Jones, S. M. G., Pinder, I. M., Moran, C. G., and Malcolm, A. J. 1992. "Polyethylene Wear in Uncemented Knee Replacements." *J. Bone Joint Surg.* 74B: 18-22.

[7] Kilgus, D. J., Moreland, J. R., Finerman, G. A., Funahashi, T. T, and Tipton, J. S. 1991. "Catastrophic Wear of Tibial Polyethylene Inserts." *Clin Orthop* 273: 223-31.

[8] Mintz, L., Tsao, A. K., McCrae, C. R., Stulberg, S., and Wright, T. 1991. "The Arthroscopic Evaluation and Characteristics of Severe Polyethylene Wear in Total Knee Arthroplasty." *Clin Orthop* 273: 215-22.

[9] Ries, M. D., Bellare, A., Livingston, B. J., Cohen, R. E., and Spector, M. 1996. "Early Delamination of a Hylamer-M Tibial Insert." *Journal of Arthroplasty* 11: 974-6.

[10] Oonishi, H., Kim, S. C., Kyomoto, M., Iwamoto, M., and Ueno, M. 2006. "PE Wear in Ceramic/PE Bearing Surface in Total Knee Arthroplasty; Clinical Experiences of More Than 24 Years." In *Proceedings of 11th BIOLOX Symposium,* 101-10.

[11] Johnson, K. L. 1985. *Contact Mechanics.* UK: Cambidge University Press

[12] Saikko, V., Ahlroos, T., and Calonius, O. 2001. "A Three Axis Wear Simulator with Ball-on-Flat Contact." *Wear* 249: 310-15.

[13] Yoshikawa, T., and Zheng, X. Z. 1993. "Coordinated Dynamic Hybrid Position/Force Control for Multiple Robot Manipulators Handling on Constrained Object." *International Journal of Robotics Research* 12 (3): 219-30.

[14] Mason, M. 1982. "Compliance and Force Control for Computer Controlled Manipulators." The MIT Press, Cambridge, MA, Ch.5, 373-404.

[15] Denavit, J., and Hartenberg, R. B. 1955. "A Kinematic Notation for Lower-Pair Mechanism Based on Matrices." *ASME J. Appl. Mechanics* 23: 215-21.

[16] Joly, L. D., Andriot, C., and Hayward, V. 1977. "Mechanical Analogic in Hybrid Position/Force Control." IEEE Albuquerque, New Mexico, 835-40.

[17] Vladareanu, L. 2003. "The Open Architecture (OAH) Control in Real Time for the Contour Robots." Presented at the AMSE 2003, International Conference of Management and Technology MT'2003, Habana, Cuba.

[18] Archard, J. F. 1953. "Contact Rubbing of Flat Surfaces." *J. Appl. Phys.* 2: 438-55.

[19] Smarandache, F., and Vladareanu, L. 2011. "Applications of Neutrosophic Logic to Robotics." In *Proceedings of The Int. Conf. on Granular Computing Kaohsiung,* 607-12.

[20] Vladareanu, V., Schiopu, P., and Vladareanu, L. 2014. "Theory and Application of Extension Hybrid Force-Position Control in Robotics." *U.P.B. Sci. Bull. Series A* 76 (3): 43-54.

[21] Vladareanu, V., Tont, G., Vladareanu, L., and Smarandache, F. 2013. "The Navigation of Mobile Robots in Non-stationary and Non-structured Environments." *Int. J. Adv. Mechatronic Systems* 5 (4): 232-43.